Available online at www.sciencedirect.com
ScienceDirect
Trans. Nonferrous Met. Soc. China 35(2025) 418−430
Transactions of Nonferrous Metals Society of China
www.tnmsc.cn

A new simple and efficient method to determine critical strain required for adiabatic shear under high-speed impact

Rui XING[1], Peng-cheng GUO[2,3], Cong-chang XU[1], De-cheng WANG[1], Luo-xing LI[1,2]

1. College of Mechanical and Vehicle Engineering, Hunan University, Changsha 410082, China;
2. Research Institute of Hunan University in Chongqing, Hunan University, Chongqing 400044, China;
3. College of Mechanical and Electrical Engineering, Central South University of Forestry and Technology, Changsha 410004, China

Received 12 July 2023; accepted 26 March 2024

Abstract: Based on the investigation of mechanical response and microstructure evolution of a commercial 7003 aluminum alloy under high-speed impact, a new simple and effective method was proposed to determine the critical strain required for the nucleation of adiabatic shear band (ASB). The deformation results of cylindrical and hat-shaped samples show that the critical strain required for ASB nucleation corresponds to the strain at the first local minimum after peak stress on the first derivative curve of true stress−true strain. The method of determining the critical strain for the nucleation of ASB through the first derivative of the flow stress curve is named the first derivative method. The proposed first derivative method is not only applicable to the 7003 aluminum alloy, but also to other metal materials, such as commercial purity titanium, WY-100 steel, and AM80 magnesium alloy. This proves that it has strong universality.

Key words: critical strain; adiabatic shear band; high-speed impact; microstructure evolution; 7003 aluminum alloy

1 Introduction

Armor, aerospace and vehicle are inevitably subjected to high-speed loads, such as high-speed collision and explosion, which often lead to adiabatic shear failure in materials, such as aluminum alloys [1], titanium alloys [2], magnesium alloys [3], steel [4], and copper [5]. The consequences of adiabatic shear failure are extremely serious, as it occurs in a very short period of time, making it difficult to predict [6,7]. To prevent this kind of disaster resulting from adiabatic shear failure, it is very necessary to accurately determine the critical strain for the nucleation of adiabatic shear band (ASB).

When the adiabatic shear occurs, large and severe plastic deformation accumulates in the ASB [8,9]. Its nucleation and propagation are the result of competition between hardening and softening [10,11]. Based on this, various theoretical calculation methods have been proposed to determine the critical condition for ASB [12−16]. RECHT [15] constructed a criterion to predict catastrophic shear, that is, the strain where the slope of the true stress−true strain curve is zero. Thermal instability is considered to be the main reason for adiabatic shear, the critical strain of which can be calculated by the method deduced by CULVER [12]. According to this method, the calculated critical strain of commercially pure titanium is 1.40, which is close to 1.15 obtained by experiment with strain rates of 105−320 s^{-1}. In addition, BAI [10] proposed a criterion based on the plastic deformation

Corresponding author: Luo-xing LI, Tel: +86-731-88821950, E-mail: luoxing_li@hnu.edu.cn
DOI: https://doi.org/10.1016/S1003-6326(24)66689-6

equation, the first law of thermodynamics, and Fourier law of heat conduction, accurately predicting the critical instability strain for simple shear deformation. It is generally accepted that the flow stress of most metal materials exhibits strain rate dependence, indicating that the loading strain rate is another factor affecting the nucleation of ASB [14,17]. To solve this problem, a critical strain model including strain rate term was constructed by PAN [14]. Moreover, the critical strain for the nucleation of ASB also depends on the heat-treated state. For peak-aged 8090 Al−Li alloy, the ASB occurs only when the applied strain rate is higher than 1600 s^{-1}, while the under-aged one requires a higher applied strain rate (2000 s^{-1}) [18]. Overall, it can be reasonably inferred that the ASB occurs only when the applied strain rate and strain are higher than the critical value.

The above methods based on theoretical calculation are essentially to determine the strain corresponding to peak stress under given deformation condition, and regard it as the critical strain for instability or adiabatic shear. However, the latest studies on commercial titanium by GUO et al [19] and aluminum alloys by KIM et al [1] have indicated that the ASB is formed after peak stress. The detected time for ASB nucleation of commercial titanium is ~9 μs after peak stress. Additionally, the detected critical strains are 58% and 38% for 2139 and 7056 aluminum alloys, respectively, and both of which are greater than the strains corresponding to the peak stress. Although the synchronized high-speed photography technique can accurately determine the critical strain for ASB nucleation, it needs to use special sample and carve grid lines on the specimen's gauge section, which is not suitable for conventional compression with cylindrical sample.

It is well known that stress response behavior is the external manifestation of the microstructure evolution [20], such as strain hardening caused by dislocation multiplication, recovery and recrystallization softening caused by dislocation annihilation, and adiabatic shear caused by local plastic instability. Accordingly, the method for predicting dynamic recrystallization based on the derivation of stress−strain curve was proposed [21], which has been widely utilized due to its simplicity, quickness, and accuracy. In this work, the nucleation and propagation of ASB were investigated with 7003 aluminum alloy. To determine the critical strain of ASB nucleation simply, quickly, and accurately, the first derivative method was proposed based on the widely used derivation method for dynamic recrystallization prediction. The content of this method is that the onset of ASB nucleation corresponds to a strain of the first local minimum after peak stress on the first derivative curve of true stress−true strain. As expected, the critical strain required for ASB nucleation in the 7003 aluminum alloy was accurately predicted by the first derivative of the true stress−true strain curve. In addition, this method was applied to other alloys to verify its adaptability.

2 Experimental

Commercial 7003 aluminum alloys, including as-extruded and as-cast states, were studied in the present study. Its chemical composition is listed in Table 1. Extrusion was carried out on an 800 t extruder with initial temperatures of 450 and 430 °C for billet and extrusion tool and an extrusion speed of 1 mm/s. The extruded 7003 bars with diameter of 12 mm were water quenched online and then naturally aged to steady state at room temperature. The as-cast ingots were solution treated at 450 °C for 16 h, then air cooled to room temperature.

Table 1 Chemical composition of 7003 aluminum alloy (wt.%)

Zn	Mg	Cu	Fe	Si	Mn
5.87	0.70	0.06	0.14	0.05	0.13
Zr	Cr	Ti	V	Al	
0.15	0.07	0.03	0.01	Bal.	

Cylindrical samples with diameter of 8 mm and height of 6 mm were cut from the natural aged extruded bar and the solution-treated ingot. Among them, the samples with two different directions (0° and 90°) to the extrusion direction (ED) were cut from the natural aging extruded bar, as shown in Fig. 1. The sample with the axis of the cylinder parallel to the extrusion direction is named 0° sample, while the sample with an axis perpendicular to the extrusion direction is named 90° sample. Hat-shaped samples were cut from the

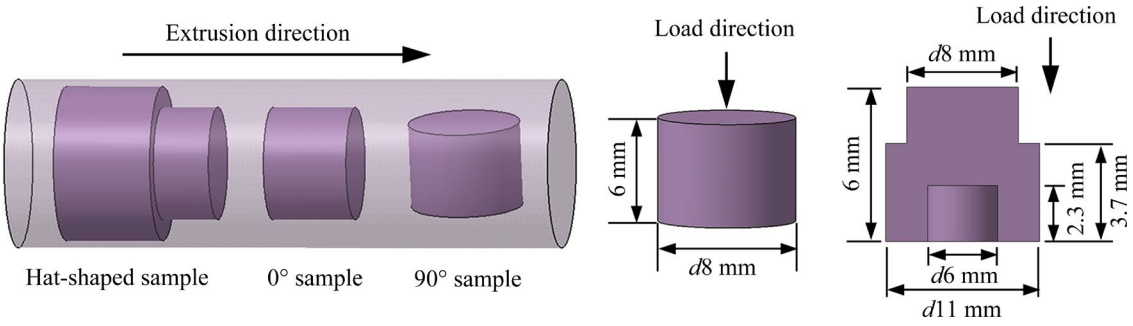

Fig. 1 Schematic diagram of samples taken from as-extruded alloy

natural aging extruded bar. Its relative position and sample size are shown in Fig. 1.

High-speed impact tests with strain rate of ~2200 s^{-1} were carried out at room temperature using a split Hopkinson pressure bar (SHPB). After impact deformation, the samples were quickly quenched by water. A series of stopper rings with an inner diameter of 28 mm and an outer diameter of 40 mm were utilized to obtain samples with specified strains. The height of rings corresponds to strains (ε) of 0.26, 0.48, and others. This method is widely used for the investigation of ASB under high-speed impact [1,9,22,23].

For microstructure analysis, the samples before and after deformation were cut using a wire-cut electrical discharge machine along the direction parallel to the load direction and through the center of the sample. Microstructure observations were performed using optical microscope (OM) and electron backscatter diffraction (EBSD). Samples used for OM observation were ground, polished, and final etched with an acid solution consisting of 5 mL HBF_4 and 195 mL H_2O. Samples for EBSD observation were ground, mechanically polished, and final ion polished with Leica EM RES102, and then characterized with an EDAX Velocity Super electron probe on a JSM 7200F scanning electron microscope at 20 kV. Hardness tests were conducted using a HV1000 Vickers hardness testing machine with load of 500 g and dwell time of 10 s.

3 Results and discussion

3.1 Method for determining critical strain of ASB nucleation

3.1.1 Results of as-extruded 0° sample

The true stress−true strain curves of the as-extruded 0° samples are shown in Fig. 2. Clearly, the consistency of three repeated impact tests is high, that is, the obtained data in this work are reliable. Overall, the stress response behavior can be simply divided into two stages. In stage 1, the flow stress increases with the increase of applied strain until the peak stress is reached at true strain of ~0.21, meaning that the plastic deformation in this stage is dominated by strain hardening until completely consumed by dynamic softening. In stage 2, the flow stress decreases continuously, indicating that softening is the main deformation characteristic in this stage. This behavior has been reported before in 7xxx aluminum alloys under high-speed impact loads [1]. Accordingly, the softening behavior detected in stage 2 is attributed to the entanglement and annihilation of dislocations caused by the increased deformation temperature [24].

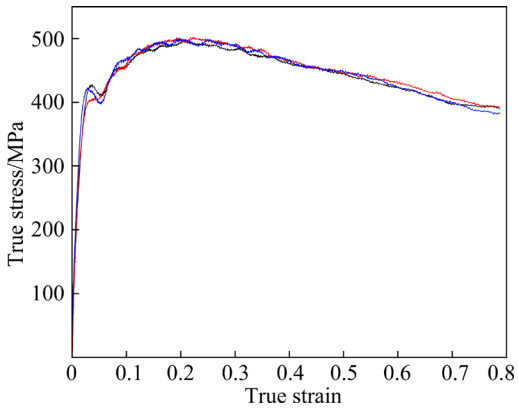

Fig. 2 True stress−true strain curves of as-extruded 0° sample at strain rate of 2200 s^{-1}

Microstructures of the as-extruded 0° sample before and after impact at 2200 s^{-1} with true strains of 0.26, 0.48, and 0.76 are shown in Fig. 3. Among them, Figs. 3(b) and (c) are half of the sections through the cylinder axis, and Figs. 3(e) and (f) are the enlarged views of Regions 1 and 2 in Fig. 3(c).

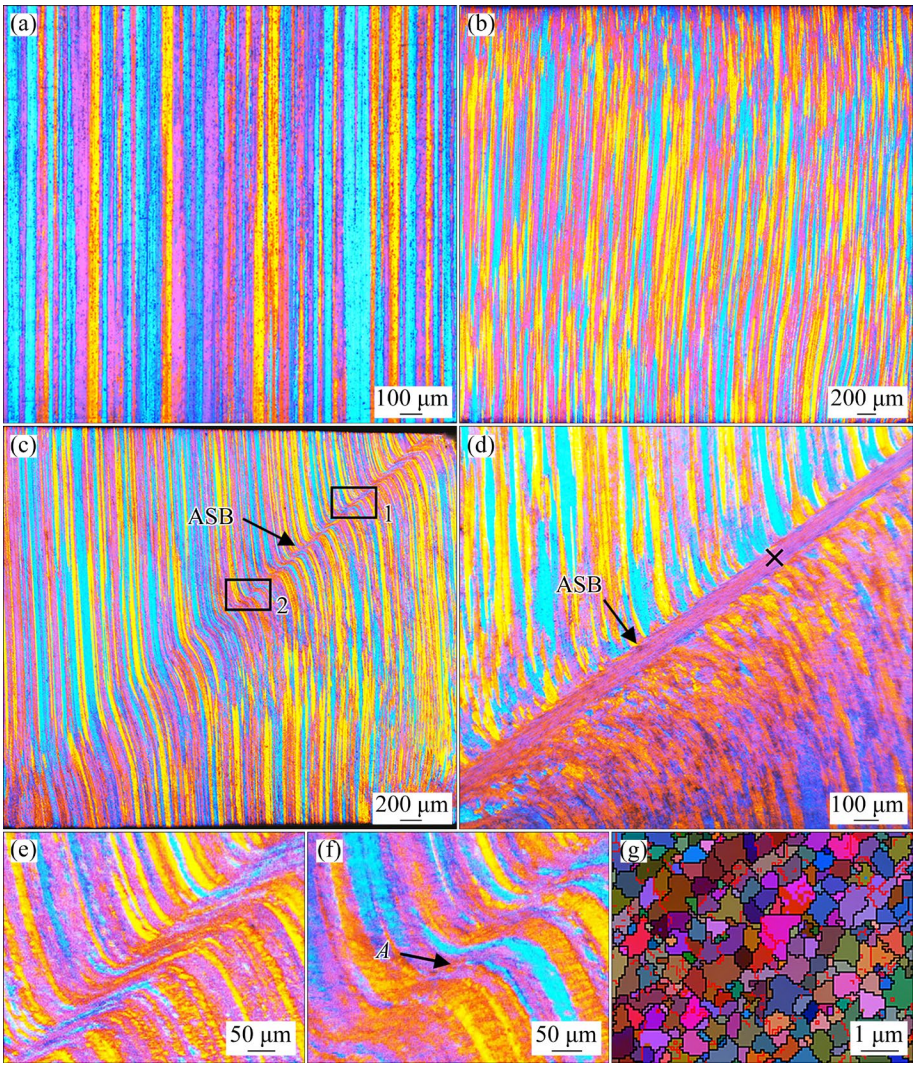

Fig. 3 Microstructures of as-extruded 0° samples before and after impact deformation at 2200 s^{-1}: (a) Undeformed state; (b) ε=0.26; (c) ε=0.48; (d) ε=0.76; (e, f) Magnified sections of Regions 1 and 2 in Fig. 3(c), respectively; (g) OIM map of cross mark in center of ASB in Fig. 3(d)

Figure 3(g) shows the orientation imaging microscopy (OIM) map of the marked region from the center of ASB in Fig. 3(d). Boundaries with angles θ>12° and 2°<θ<12° are represented with black lines and red lines, respectively. Before impact deformation, the fibrous grains are parallel to ED, with average size of 25 μm. At true strain of 0.26, the deformed microstructure is still fibrous with direction parallel to ED. Additionally, no ASB is detected. As the applied true strain increases to 0.48, an ASB with length of ~2.5 mm and width of ~42 μm is observed, as shown in Fig. 3(c). It is worth noting that the detected ASB propagates along the direction of shear deformation, which is approximately 45° away from the impact direction. As a result, the fibrous grains in the shear direction are clearly distorted and stretched into an N shape, as shown in Fig. 3(e). Moreover, the fibrous grains at the tip of ASB have evolved into S shape, whose boundaries are hard to distinguish, as shown in Fig. 3(f). According to the calculation method in Refs. [25,26], the average shear strain in the ASB is obtained as 4.5. When the impacted true strain continues to increase to 0.76, an ASB with a width of ~74 μm is clearly observed throughout the impacted sample, while the grains outside the ASB remain fibrous. As shown in Fig. 3(g), the microstructure in the center of ASB is composed of equiaxed grains with average size of 477 nm, which further confirms that adiabatic shear occurs in the as-extruded 7003 alloy during high-speed impact deformation.

The ASB occurs only when a critical strain is reached, which depends on deformation conditions, such as temperature, strain rate, and heat treatment state [14,15,18]. Essentially, the competition between strain hardening and thermal softening is considered to be the inducement for the nucleation and propagation of ASBs [10,11]. As shown in Fig. 3, there is no ASB at the strain of 0.26, while a fine ASB occurs as the applied strain increases to 0.48, which indicates that the critical strain of the as-extruded 7003 alloy is between 0.26 and 0.48.

3.1.2 First derivative method

Essentially, the competition between strain hardening and thermal softening is considered to be the inducement for the nucleation and propagation of ASBs [10,11]. Internal energy dissipation is always associated with plastic deformation. The consumed energy is converted into heat or induces permanent changes in microstructure, both of which are irreversible processes [27]. Accordingly, POLIAK and JONAS [21] proposed that when the internal state variable satisfies Eq. (1), the internal dissipation rate of materials reaches a steady state, which is considered to be the critical point of instability.

$$\sum_j \frac{\partial}{\partial X_k}\left(\frac{A_j^{\mathrm{c}}\dot{\xi}_j^{\mathrm{c}}}{T}\right)-\sum_j \frac{A_j^{\mathrm{c}}}{T}\frac{\partial \dot{\xi}_j^{\mathrm{c}}}{\partial X_k}=0 \tag{1}$$

where ξ_j is the internal dissipative variable with thermodynamically conjugate affinity A_j, X_k is a set of generalized forces acting within system, and T is the temperature. To facilitate analysis, Eq. (1) is simplified by considering only one parameter of hardness. In this case, the internal variable can be related to the strain by the following equations:

$$\theta=\left(\frac{\partial \sigma^*}{\partial \varepsilon}\right)_{\dot{\varepsilon}}=A \tag{2}$$

$$P_{\mathrm{d}}=\theta\dot{\varepsilon} \tag{3}$$

where θ is the hardening rate, σ^* is the internal stress, ε is the strain, P_{d} is the dissipation power, and $\dot{\varepsilon}$ is the strain rate. Thereby, Eq. (1) can be reduced to Eq. (4) when applied an external stress σ.

$$\dot{\varepsilon}\frac{\partial \theta}{\partial \sigma}=0 \tag{4}$$

This indicates that the internal state of material reaches a dynamic equilibrium at the extreme value of hardening rate, and then instability may occur as deformation continues. For high-speed impact deformation, thermoplastic instability induced by adiabatic shear is one of the signs of material instability [15]. In addition, flow stress is the external manifestation of plastic deformation [28]. As one of the external manifestations of microstructure evolution, strain hardening rate (SHR) is widely used in the research of deformation behavior and deformation mechanisms [9,21,29,30]. Therefore, it is feasible to determine the critical strain required for adiabatic shear instability based on the extreme value of SHR. The method to determine the critical strain of ASB based on SHR curve is named the first derivative method in this work.

3.1.3 Determination of critical strain for ASB nucleation

To facilitate the subsequent calculation and analysis, it is necessary to smooth the collected data with many burrs. Accordingly, the polynomial order required for fitting the entire flow stress curve is 11 or higher [31]. Here, one of the curves in Fig. 2 was selected and fitted using 14th-order polynomial, as shown in Fig. 4. Clearly, the fitted stress−strain curve is in good agreement with the experimental result. The relationship between SHR and true strain was then obtained by solving the first derivative of the fitted curve, as shown in Fig. 4. The strain corresponding to the first local minimum of the SHR curve after peak stress is 0.33, which is considered the critical strain for the nucleation of ASB based on the above analysis. To verify this assumption, a stopper ring with a height of 4.3 mm was designed to obtain the specified strain of 0.33. The OM image with true strain of 0.33 at 2200 s^{-1} is shown in Fig. 5. As expected, an ASB with length of ~0.45 mm and width of ~22 μm is observed, indicating that the ASB has nucleated and even slightly propagated at this moment. There is a slight deviation in using this strain as the critical strain for ASB nucleation, indicating a slight deviation in determining the critical strain using the first derivative method. This can be attributed to factors such as manual measurements, data acquisition from experimental equipment, and data processing. However, for high-speed impact tests, such slight deviation can be basically ignored. Consequently, it can be concluded that the strain corresponding to the first local minimum of SHR curve after peak stress is the critical strain for the nucleation of ASB.

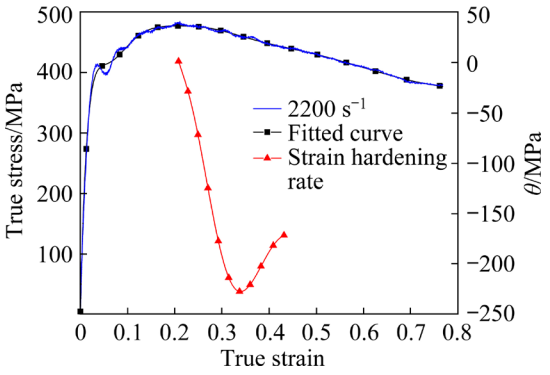

Fig. 4 Original and fitted true stress−true strain and SHR (θ)−true strain curves of as-extruded 0° sample (θ=dσ/dε)

The local minimum of SHR curve represents transformation of the plastic deformation mechanism [9]. To reveal the inducement for the increase of SHR after instability, the microhardness distribution on the sections as that for microstructure characterization in Fig. 3 is shown in Fig. 6. As expected, the microhardness distribution of the undeformed sample is basically uniform. As the impacted strain increases to 0.26, the microhardness apparently increases, with maximum and average harnesses of $HV_{0.5}$ 153.5 and $HV_{0.5}$ 143.8, respectively. In contrast, the microhardness on the top is slightly higher than that on the bottom. The reason for the uneven distribution of microhardness is due to the fact that, under high-speed impact load, the deformation of sample starts from the side close to transmitter bar, causing the deformation of this region to occur before other regions, especially the region far from transmitter bar [29].

When the impacted strain increases to 0.48, the microhardness of the adiabatic shear region corresponding to Fig. 3(c) increases significantly, which is much higher than that of the surrounding non-shear regions. According to the research by YANG et al [32], the significant increase in microhardness during adiabatic shearing is attributed to the rapid multiplication of dislocations, which leads to a significant increase in dislocation density, resulting in dislocation tangles and even dislocation cell structure. In sharp contrast, the microhardness far from the shear band remains almost the same. Combined with the OM results in Fig. 3, it can be inferred that most of plastic deformation in this stage is concentrated in the shear region, resulting in the strain hardening here being higher than the thermal softening caused by adiabatic temperature rise, so the SHR increases after plastic instability.

At present, the critical strain of ASB is generally determined through theoretical calculation [10,12,14,16]. According to the assumption that ASB nucleates at the strain corresponding to the maximum stress, CULVER [12] proposed a critical strain criterion based on the constructed constitutive model of $\tau=K\gamma^n$. The critical shear strain γ_c for ASB nucleation can be calculated using the following equation:

$$\gamma_c=\frac{n\rho C_v}{\alpha} \tag{5}$$

where n is strain hardening exponent, α is thermal softening rate, and ρ and C_v are density and specific heat capacity, respectively. The true strain ε can be

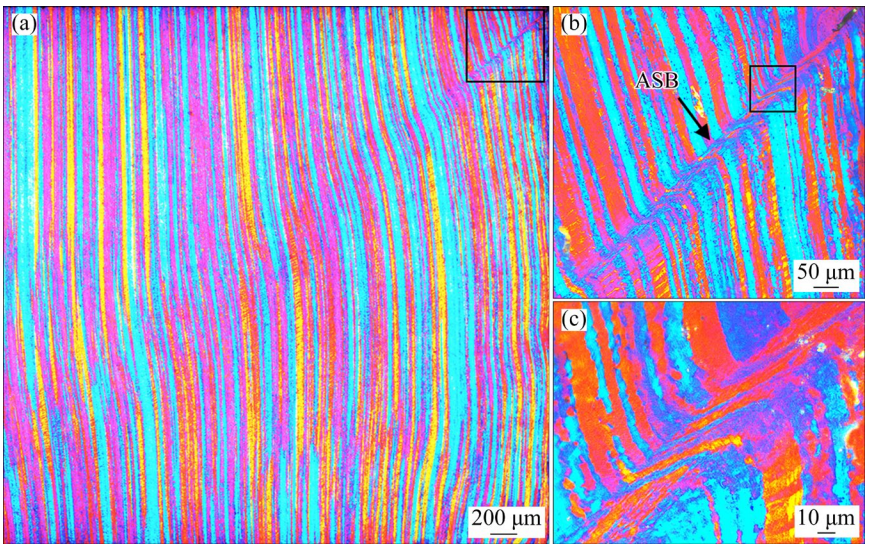

Fig. 5 (a) OM image of as-extruded 0° sample with true strain of 0.33 at 2200 s^{-1}; (b, c) Magnified sections of regions in Figs. 5(a) and (b), respectively

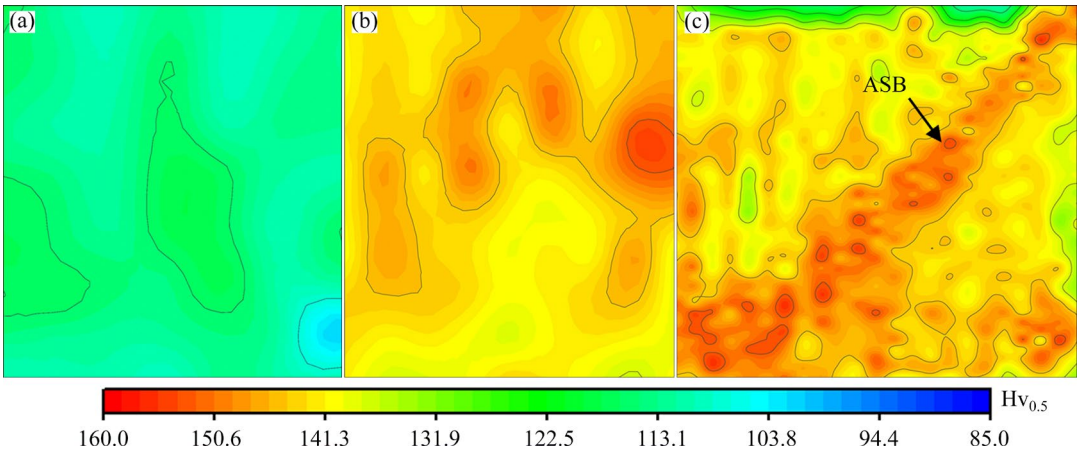

Fig. 6 Contour plots of microhardness distribution of as-extruded 0° sample before and after impact at 2200 s^{-1}: (a) ε=0; (b) ε=0.26; (c) ε=0.48

calculated with shear strain γ by the following equation [12]:

$$\varepsilon=\ln\sqrt{1+\gamma+\gamma^2/2} \quad (6)$$

For the as-extruded 7003 alloy, the strain hardening exponent n and thermal softening rate α calculated from its true stress−true strain curve are 0.289 and 0.807 MPa/K, respectively. Additionally, its density and specific heat capacity are 2.7×10^3 kg/m^3 and 875 J/(kg·K). Thereby, the critical strain for the nucleation of ASB is obtained as 0.39. It is worth noting that the critical strain obtained by theoretical calculation is clearly higher than that (0.33) calculated by the first derivative method. This deviation is mainly caused by two aspects. Firstly, the theoretical calculation criterion is proposed based on the assumption that plastic instability occurs at peak stress. Secondly, some conditions, such as strain rate, are ignored in order to simplify the derivation. For the first derivative method, the true stress−true strain curve, which can macroscopically characterize the microstructure evolution, is directly used to derive the critical strain for the nucleation of ASB. This is considered to be the main reason for its high accuracy.

3.2 Applicability of method in 7003 alloy

3.2.1 As-extruded 90° sample

Figures 7 and 8 illustrate the true stress−true strain curves and the corresponding deformed microstructure of the as-extruded 90° sample under strain rate of 2250 s^{-1}. As shown in Fig. 7, the flow stress increases with increasing applied strain until it reaches peak stress at true strain of approximately

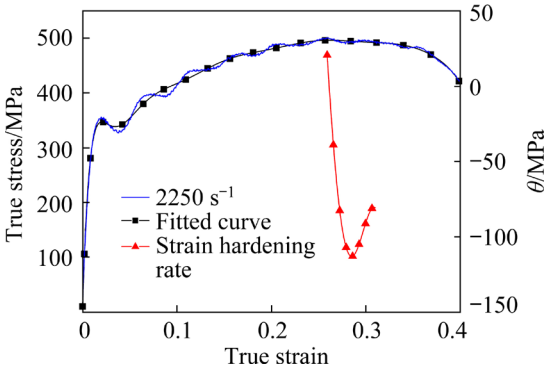

Fig. 7 Curves of original and fitted true stress−true strain and SHR(θ)−true strain of as-extruded 90° sample

0.25. Beyond this point, the stress decreases as the strain continues to increase. Before compression, the microstructure of the 90° sample consists of equiaxed grains with an average size of 40 μm, as shown in Fig. 8(a). Figure 8(b) reveals that even after deforming the sample to a strain of 0.16, the grains remain equiaxed, with little significant deformation observed even at the sample's edge (upper right corner in Fig. 8(b)). However, the ASB with a width of ~38 μm becomes evident in the sample subjected to a strain of 0.4 (Fig. 8(c)). This indicates that, similar to the 0° sample, the 90° sample also exhibits a notable adiabatic shear phenomenon during high-speed impact.

To estimate the critical strain for ASB nucleation, a 14th-order polynomial was employed to fit the true stress−true strain curve. The fitted curves of true stress−true strain and SHR−true strain for the as-extruded 90° sample are displayed in Fig. 7. The critical strain for ASB nucleation, determined using the first derivative method, is

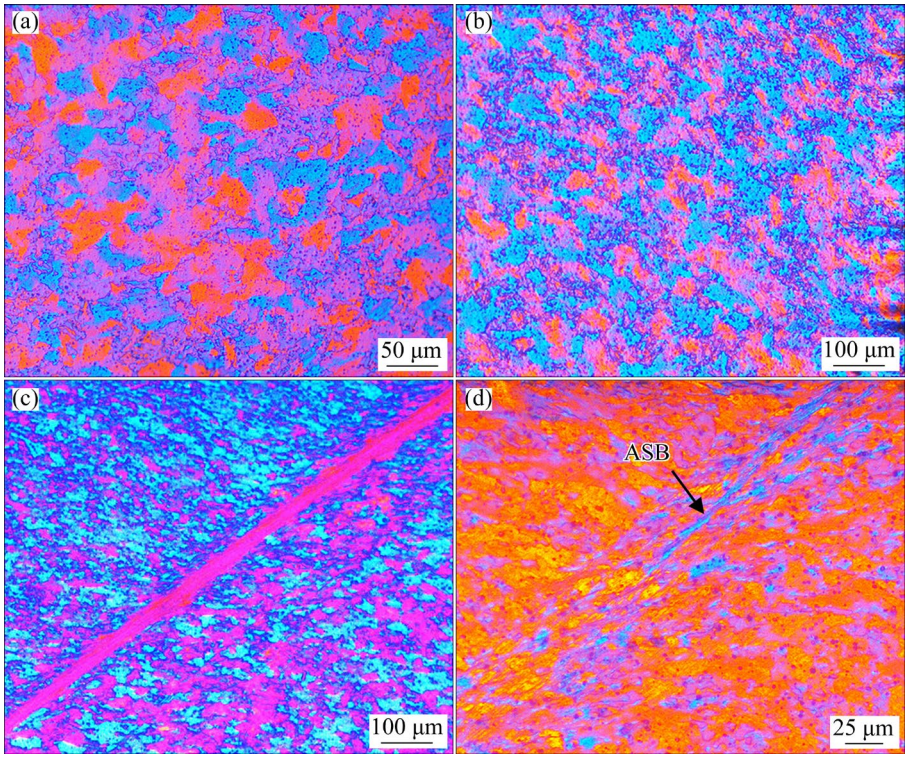

Fig. 8 OM images of as-extruded 90° sample at 2250 s^{-1}: (a) Undeformed state; (b) ε=0.16; (c) ε=0.40; (d) ε=0.28

determined to be 0.28. In order to reach a sample with strain of 0.28, a stopper ring with height of 4.5 mm was designed and implemented in the high-speed impact test. Figure 8(d) exhibits the microstructure at true strain of 0.28 and strain rate of 2250 s^{-1}. The ASB with length of ~0.18 mm and width of ~4 μm is observed in the upper right corner of the sample, indicating that the ASB has just nucleated at strain of 0.28. The predicted result obtained from the first derivative method is fairly consistent with the experimental result, demonstrating the reliability of this approach.

3.2.2 As-cast 7003 alloy

To verify the adaptability of the first derivative method, high-speed impact tests at 2150 s^{-1} were carried out with the as-cast 7003 alloy in solution-treated state. The true stress−true strain curve and the corresponding deformed microstructure of the as-cast 7003 alloy are shown in Figs. 9 and 10, respectively. As shown in Fig. 9, the flow stress reaches its peak stress at true strain of ~0.3 and then decreases with increasing strain. Clearly, the undeformed grains of as-cast 7003 alloy are equi-axed with average size of ~153 μm. As the strain increases to 0.76, the ASB with width of ~56 μm penetrates the entire sample, which indicates that the ASB has been propagated sufficiently in the

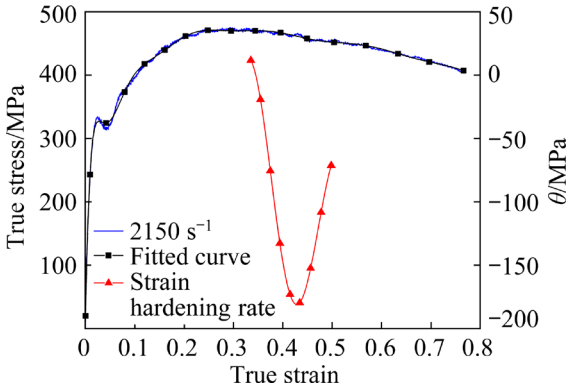

Fig. 9 Curves of original and fitted true stress−true strain and SHR(θ)−true strain of as-cast 7003 alloy

as-cast 7003 alloy. The curves of fitted true stress−true strain and SHR−true strain are shown in Fig. 9. The critical strain for the nucleation of ASB calculated by the first derivative method is 0.43, which corresponds to a stopper ring with height of 3.9 mm. The OM image with true strain of 0.43 at 2150 s^{-1} is shown in Fig. 10(b). As expected, a fine ASB with length of ~0.3 mm and width of ~25 μm is detected on the top right corner, illustrating that the ASB has just been nucleated at the true strain of 0.43. Therefore, the first derivative method proposed here can also be utilized to predict the critical strain of ASB for the as-cast 7003 alloy.

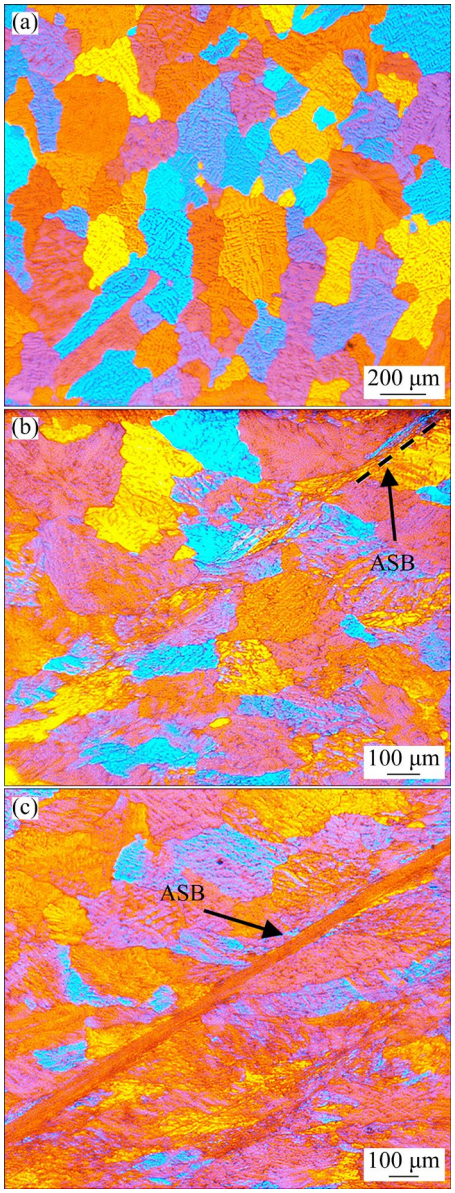

Fig. 10 OM images of as-cast 7003 alloy at 2150 s^{-1}: (a) Undeformed state; (b) ε=0.43; (c) ε=0.76

The critical strain for the nucleation of ASB in as-extruded samples is determined to be smaller compared to the as-cast samples at basically the same strain rate. For the as-extruded samples, the ASB nucleation critical strain of the 90° sample is less than that of the 0° sample, which has also been observed in other study [30]. As reported, this difference is attributed to the anisotropy, resulting from texture, grain morphology, grain size, precipitates, and other factors [33,34]. As is well known, there is fiber texture in materials formed by extrusion, which leads to anisotropy of as-extruded samples. The plastic strain anisotropy of materials can be quantified by the strain ratio, r [35], which provides information about the uniformity of plastic deformation in a material. A higher r value indicates more uniform plastic deformation. For isotropic materials, multiple slip occurs inside the material during plastic deformation, with r close to 1, which promotes uniform deformation of the sample and resists the nucleation of shear bands [33]. For materials with strong texture, the Schmidt factors in different directions are different, which leads to low r values. A low r value indicates that the sample exhibits non-uniform plastic deformation under high-speed impact loads, promoting the occurrence of shear localization [34].

3.2.3 Hat-shaped samples of as-extruded 7003 alloy

In addition to cylindrical samples, hat-shaped samples are also commonly used to investigate the initiation and evolution of ASBs [8]. In this study, high-speed impact tests were conducted at strain rate of 2150 s^{-1} using hat-shaped samples made of the as-extruded 7003 alloy. The true stress−true strain curve and the corresponding deformed microstructure are presented in Figs. 11 and 12, respectively. As shown in Fig. 11, similar to the cylindrical sample, the true stress of the hat-shaped sample gradually increases until it reaches its peak value at true strain of ~0.06, after which it decreases during the impact process. At true strain of 0.14, a well-developed ASB with width of ~20 μm running through the sample can be clearly observed (Fig. 12(a)).

To estimate the critical strain for ASB nucleation, the first derivative method was applied. In order to obtain a smooth curve, the original true stress−true strain curve was fitted. Then, the first derivative of the fitted curve was calculated to obtain the SHR curve. Figure 11 depicts the curves

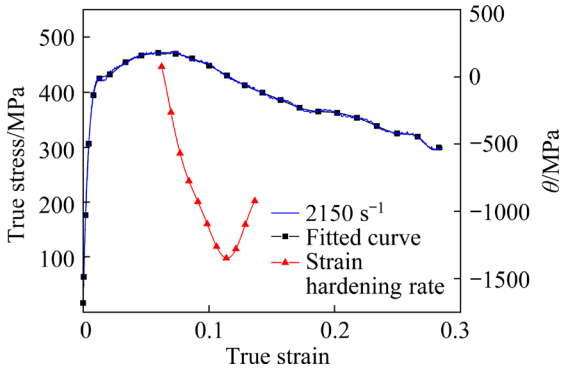

Fig. 11 Curves of original and fitted true stress−true strain and SHR(θ)−true strain of hat-shaped sample of as-extruded 7003 alloy

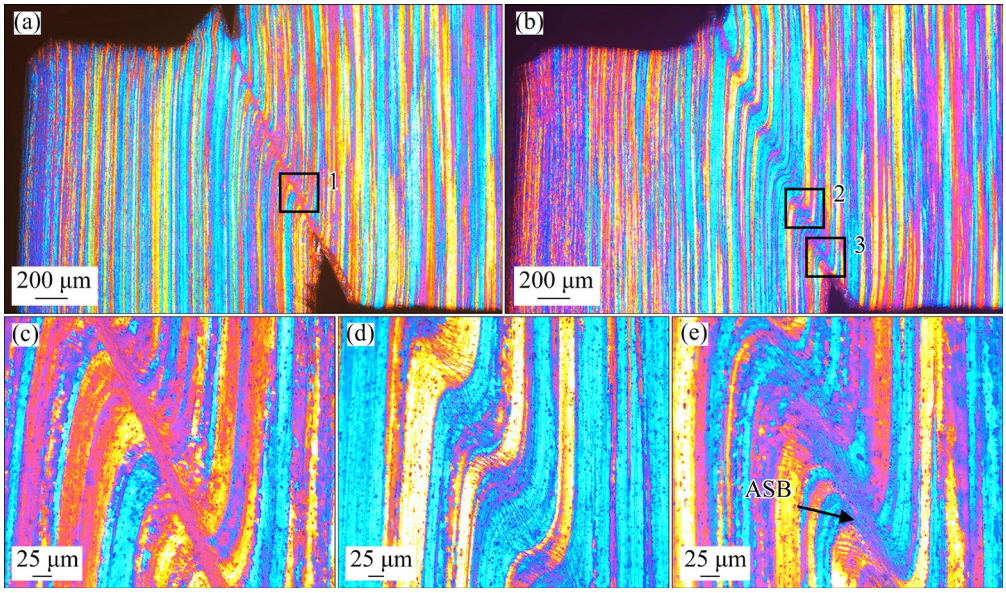

Fig. 12 OM images of hat-shaped samples of as-extruded 7003 alloy at 2150 s^{-1}: (a) ε=0.14; (b) ε=0.12; (c, d, e) Enlarged images of Regions 1, 2 and 3 in Figs. 12(a) and (b), respectively

of the fitted true stress−true strain and SHR. The minimum value of the SHR curve occurs at a strain of 0.12, indicating that the critical strain for ASB nucleation is determined to be 0.12. To obtain a sample with strain of 0.12, a stopper ring with height of 5.3 mm was designed and utilized in the high-speed impact test. The microstructure corresponding to true strain of 0.12 at strain rate of 2150 s^{-1} is displayed in Fig. 12(b). An ASB with length of ~0.16 mm is observed. The maximum relative displacement of deformed grains within the ASB in the shear direction is approximately 88 μm (Fig. 12(e)). Outside of the ASB, the deformed grains undergo torsion without relative displacement in the shear direction (Fig. 12(d)). In the case of pure shear samples, these observations indicate that the ASB has just nucleated and is developing along the shear direction. These findings are well consistent with the estimation results of the first derivative method, suggesting the applicability of this method to hat-shaped samples as well.

3.3 Applicability of method to other metal materials

To further explore the adaptability of the first derivative method, it is extended to calculate the critical strain of ASB for other mental materials. In this paper, these investigations on adiabatic shear band nucleation using high-speed cameras [36−38] or interrupted impact test methods [1,29,39,40] were selected to verify the proposed method. The critical strains of ASB nucleation obtained by high-speed photography technology are 0.63 for the commercial purity titanium at 13000 s^{-1} [36], 0.40 for the WY-100 steel at 1600 s^{-1} [37], and 0.67 for the 603 armor steel at 14000 s^{-1} [38]. The critical strain of ASB nucleation determined by microstructure analysis is in the range of 0.20−0.25 for the AM80 magnesium alloy at 5000 s^{-1} [39], 0.28 for the high-strength armor steel at impact momentum of 16.3 kg·m/s [40], 0.38 for the 7056 aluminum alloy at impact momentum of 16 kg·m/s [1], and 0.47 for the AA2017-T451 at 5340 s^{-1} [29].

Here, the first derivative method was used to determine the critical strain of ASB nucleation in these materials. To obtain the SHR curves, the coordinates of each point before and after peak stress were extracted. Subsequently, the smooth stress−strain curve and the relationship curve between SHR and true strain were obtained using the methods of polynomial fitting and derivation, respectively, as depicted in Fig. 13. In this way, the strains corresponding to the first local minimum of the SHR curve after peak stress were obtained, as shown in Table 2. Remarkably, the strains calculated by the first derivative method are extremely consistent with the critical strain for the nucleation of ASB obtained by experiments. This consistency indicates that the first derivative method is also applicable to other metallic materials.

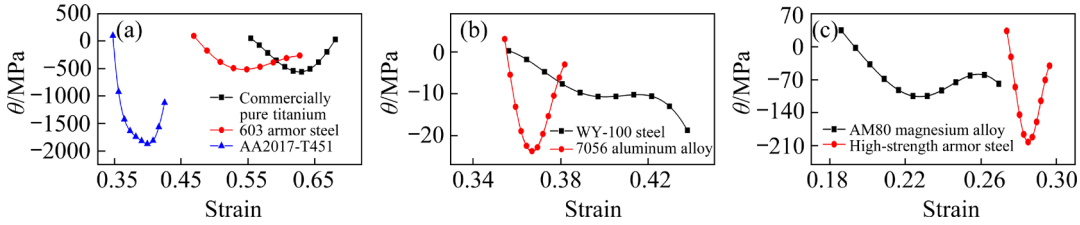

Fig. 13 SHR(θ)−strain curves of other metal materials

Table 2 Critical strain for nucleation of ASB in other metal materials

Material	Experiment condition	Critical strain	
		Experiment	First derivative method
Commercially pure titanium [36]	13000 s^{-1}	0.63	0.627
WY-100 steel [37]	1600 s^{-1}	0.40	0.400
AM80 magnesium alloy [39]	5000 s^{-1}	0.2−0.25	0.227
High-strength armor steel [40]	16.3 kg·m·s^{-1}	0.28	0.285
7056 aluminum alloy [1]	16 kg·m·s^{-1}	0.38	0.368
603 armor steel [38]	14000 s^{-1}	0.67	0.542
AA2017-T451 [29]	5340 s^{-1}	0.47	0.402

4 Conclusions

(1) At strain rate of about 2200 s^{-1}, the critical strains for ASB nucleation determined by the first derivative method are 0.33 for the as-extruded 0° sample, 0.28 for the as-extruded 90° sample, 0.43 for the as-cast 7003 alloy, and 0.12 for the hat-shaped sample of the as-extruded 7003 alloy. The experimental results are quite consistent with the predicted results of the first derivative method.

(2) The critical strain for ASB nucleation in as-cast samples is greater than that in as-extruded samples. This disparity can be attributed to the presence of strong texture in the as-extruded samples, which leads to anisotropy in the plastic deformation behavior.

(3) The first derivative method for predicting the critical strain of ASB nucleation under high-speed impact is highly adaptable. In addition to the 7003 aluminum alloy, the method is also suitable for other metal materials.

CRediT authorship contribution statement

Rui XING: Writing − Original draft, Validation, Methodology, Investigation, Formal analysis, Data curation, Conceptualization; **Peng-cheng GUO:** Writing − Review & editing, Supervision, Project administration; **Cong-chang XU:** Resources, Project administration, Funding acquisition; **De-cheng WANG:** Supervision, Project administration; **Luo-xing LI:** Writing − Review & editing, Resources, Funding acquisition, Conceptualization.

Declaration of competing interest

The authors declare that they have no known competing financial interests or personal relationships that could have appeared to influence the work reported in this paper.

Acknowledgments

The authors gratefully acknowledge the financial support from the National Natural Science Foundation of China (No. U20A20275), and Natural Science Foundation of Hunan Province, China (No. 2021JJ40096).

References

[1] KIM S, JO M C, PARK T W, HAM J, SOHN S S, LEE S. Correlation of dynamic compressive properties, adiabatic shear banding, and ballistic performance of high-strength 2139 and 7056 aluminum alloys [J]. Materials Science and Engineering A, 2021, 804: 140757.

[2] ZHU Xin-jie, FAN Qun-bo, WANG Duo-duo, GONG

Hai-chao, GAO Yu, QIAN Feng, JIN Shen-bao, SHA Gang. A new dynamic recrystallization mechanism in adiabatic shear band of an α/β dual phase titanium alloy: Composition redistribution [J]. Scripta Materialia, 2022, 206: 114229.

[3] WANG Xue-zhao, WANG You-qiang, NI Chen-bing, FANG Yu-xin, YU Xiao, ZHANG Ping. Effect of Gd content on microstructure and dynamic mechanical properties of solution-treated Mg−xGd−3Y−0.5Zr alloy [J]. Transactions of Nonferrous Metals Society of China, 2022, 32: 2177−2189.

[4] LI Xian-yu, ZHANG Zhao-hui, CHENG Xing-wang, WANG Qiang, JIA Xiao-tong, WANG Dan, WANG Xin-fu. The evolution of adiabatic shear band in high Co−Ni steel during high strain-rate compression [J]. Materials Science and Engineering A, 2022, 858: 144173.

[5] BOAKYE-YIADOM S, BASSIM N. Microstructural evolution of adiabatic shear bands in pure copper during impact at high strain rates [J]. Materials Science and Engineering A, 2018, 711: 182−194.

[6] YANG Yang, JIANG Li-hong. Self-organization of adiabatic shear bands in ZK60 Magnesium alloy [J]. Materials Science and Engineering A, 2016, 655: 321−330.

[7] TIMOTHY S P, HUTCHINGS I M. The structure of adiabatic shear bands in a titanium alloy [J]. Acta Metallurgica, 1985, 33: 667−676.

[8] DU Yu-xuan, YANG Xin-liang, LI Zu-shu, HAO Fang, MAO You-chuan, LI Shao-qiang, LIU Xiang-hong, FENG Yong, YAN Zhi-ming. Shear localization behavior in hat-shaped specimen of near-α Ti−6Al−2Zr−1Mo−1V titanium alloy loaded at high strain rate [J]. Transactions of Nonferrous Metals Society of China, 2021, 31: 1641−1655.

[9] GUO Peng-cheng, LIU Xiao, ZHU Bi-wu, LIU Wen-hui, ZHANG Li-qiang. The microstructure evolution and deformation mechanism in a casting AM80 magnesium alloy under ultra-high strain rate loading [J]. Journal of Magnesium and Alloys, 2022, 10: 3205−3216.

[10] BAI Yi-long. Thermo-plastic instability in simple shear [J]. Journal of the Mechanics and Physics of Solids, 1982, 30: 195−207.

[11] WRIGHT T W, WALTER J W. Stress collapse in adiabatic shear bands [J]. Journal of the Mechanics and Physics of Solids, 1987, 35: 701−720.

[12] CULVER R S. Metallurgical effects at high strain rates [M]. New York: Plenum Press, 1973: 519−530.

[13] BURNS T J, TRUCANO T G. Instability in simple shear deformations of strain-softening materials [J]. Mechanics of Materials, 1982, 1: 313−324.

[14] PAN J. Perturbation analysis of shear strain localization in rate sensitive materials [J]. International Journal of Solids and Structures, 1983, 19: 153−164.

[15] RECHT R F. Catastrophic thermoplastic shear [J]. Journal of Applied Mechanics, 1964, 31: 189−193.

[16] CLIFTON R J, DUFFY J, HARTLEY K A, SHAWKI T G. On critical conditions for shear band formation at high strain rates [J]. Scripta Metallurgica, 1984, 18: 443−448.

[17] LEE W S, TANG Z C. Relationship between mechanical properties and microstructural response of 6061-T6 aluminum alloy impacted at elevated temperatures [J]. Materials & Design, 2014, 58: 116−124.

[18] XU Y B, ZHONG W L, CHEN Y J, SHEN L T, LIU Q, BAI Y L, MEYERS M A. Shear localization and recrystallization in dynamic deformation of 8090 Al−Li alloy [J]. Materials Science and Engineering A, 2001, 299: 287−295.

[19] GUO Ya-zhou, RUAN Qi-chao, ZHU Sheng-xin, WEI Q, CHEN Hao-sen, LU Jia-nan, HU Bo, WU Xi-hui, LI Yu-long, FANG Dai-ning. Temperature rise associated with adiabatic shear band: Causality clarified [J]. Physical Review Letters, 2019, 122: 015503.

[20] LIU Xiao, JONAS J J, LI Luo-xing, ZHU Bi-wu. Flow softening, twinning and dynamic recrystallization in AZ31 magnesium [J]. Materials Science and Engineering A, 2013, 583: 242−253.

[21] POLIAK E I, JONAS J J. A one-parameter approach to determining the critical conditions for the initiation of dynamic recrystallization [J]. Acta Materialia, 1996, 44: 127−136.

[22] MA Zi-hao, HOU Bing, QIN Dong-yang, LI Yu-long. Effect of strain rate on mechanical properties of HCP/FCC dual-phase $CoCrFeNiNb_{0.5}$ high-entropy alloy [J]. Transactions of Nonferrous Metals Society of China, 2023, 33: 1144−1155.

[23] GUO Peng-cheng, LI Luo-xing, XIAO Gang, CAO Shu-fen, WANG Guan, HE Hong. High-speed impact behavior of a casting AM80 magnesium alloy under various deformation temperatures [J]. Journal of Alloys and Compounds, 2019, 811: 151875.

[24] YE Tuo, LI Luo-xing, GUO Peng-cheng, XIAO Gang, CHEN Zi-ming. Effect of aging treatment on the microstructure and flow behavior of 6063 aluminum alloy compressed over a wide range of strain rate [J]. International Journal of Impact Engineering, 2016, 90: 72−80.

[25] XU Yong-bo, BAI Yi-long, MEYERS M A. Deformation, phase transformation and recrystallization in the shear bands induced by high-strain rate loading in titanium and its alloys [J]. Journal of Materials Science & Technology, 2006, 22: 737−746.

[26] WRIGHT T W, PERZYNA P. Physics and mathematics of adiabatic shear bands [J]. Applied Mechanics Reviews, 2003, 56: B41−B43.

[27] HUANG Bao-zong. Tensor and continuum mechanics [M]. Beijing: Metallurgical Industry Press, 2012. (in Chinese)

[28] PRASAD G V S S, GOERDELER M, GOTTSTEIN G. Work hardening model based on multiple dislocation densities [J]. Materials Science and Engineering A, 2005, 400: 231−233.

[29] TIAMIYU A A, BADMOS A Y, ODESHI A G. Effects of temper condition on high strain-rate deformation of AA 2017 aluminum alloy in compression [J]. Materials & Design, 2016, 89: 872−883.

[30] TIAMIYU A A, ODESHI A G, SZPUNAR J A. Crash-worthiness of a recently-developed AA 2624 aluminum alloy: Experimental studies [J]. Materials Science and Engineering A, 2019, 766: 138389.

[31] JONAS J J, GHOSH C, QUELENNEC X, BASABE V V. The critical strain for dynamic transformation in hot deformed austenite [J]. ISIJ International, 2013, 53: 145−151.

[32] YANG Y, JIANG L H, LUO S H, HU H B, TANG T G, ZHANG Q M. Effect of strain on microstructure evolution of

1Cr18Ni9Ti stainless steel during adiabatic shearing [J]. Journal of Materials Engineering and Performance, 2016, 25: 29−37.

[33] BHATTACHARYYA J J, AGNEW S R, LEE M M, WHITTINGTON W R, EL KADIRI H. Measuring and modeling the anisotropic, high strain rate deformation of Al alloy, 7085, plate in T711 temper [J]. International Journal of Plasticity, 2017, 93: 46−63.

[34] ZHANG Wei-liang, CHEN Xin-feng, ZHOU Bo-chen, LI Pei-jie, HE Liang-ju. Effect of strain rate and temperature on dynamic mechanical behavior and microstructure evolution of ultra-high strength aluminum alloy [J]. Materials Science and Engineering A, 2018, 730: 336−344.

[35] TRUSZKOWSKI W. The plastic anisotropy in single crystals and polycrystalline metals [M]. Netherlands: Springer, 2001.

[36] GUO Ya-zhou, RUAN Qi-chao, ZHU Sheng-xin, WEI Q, LU Jia-nan, HU Bo, WU Xi-hui, LI Yu-long. Dynamic failure of titanium: Temperature rise and adiabatic shear band formation [J]. Journal of the Mechanics and Physics of Solids, 2020, 135: 103811.

[37] MARCHAND A, DUFFY J. An experimental study of the formation process of adiabatic shear bands in a structural steel [J]. Journal of the Mechanics and Physics of Solids, 1988, 36: 251−283.

[38] XU Ze-jian, LIU Yu, SUN Zhong-yue, HU Hong-zhi, HUANG Feng-lei. On shear failure behaviors of an armor steel over a large range of strain rates [J]. International Journal of Impact Engineering, 2018, 118: 24−38.

[39] GUO Peng-cheng. The dynamic mechanical response and failure behavior of AM80 magnesium alloy at various temperatures [D]. Changsha: Hunan University, 2017. (in Chinese)

[40] JO M C, KIM S, KIM D W, PARK H K, HONG S S, KIM H K, KIM H S, SOHN S S, LEE S. Understanding of adiabatic shear band evolution during high-strain-rate deformation in high-strength armor steel [J]. Journal of Alloys and Compounds, 2020, 845: 155540.

一种简单有效确定高速冲击下绝热剪切临界应变的新方法

邢 瑞[1]，郭鹏程[2,3]，徐从昌[1]，王德成[1]，李落星[1,2]

1. 湖南大学 机械与运载工程学院，长沙 410082；
2. 湖南大学 重庆研究院，重庆 400044；
3. 中南林业科技大学 机电工程学院，长沙 410004

摘 要：基于对商用 7003 铝合金在高速冲击下的力学响应和显微组织演变的研究，提出一种简单有效的新方法来确定绝热剪切带(ASB)成核所需的临界应变。圆柱形和帽形样品的变形结果表明，ASB 成核的临界应变对应真应力−真应变的一阶导数曲线上峰值应力后的第一个局部最小值。将这种通过流动应力曲线的一阶导数确定 ASB 成核临界应变的方法命名为一阶导数法。所提出的一阶导数法不仅适用于 7003 铝合金，也可用于其他金属材料，如商业纯钛、WY-100 钢和 AM80 镁合金等。这证明一阶导数法具有很强的普适性。

关键词：临界应变；绝热剪切带；高速冲击；显微组织演变；7003 铝合金

(Edited by Xiang-qun LI)